

Manifold constrained steepest descent

Kaiwei Yang¹ Lexiao Lai¹

Abstract

Norm-constrained linear minimization oracle (LMO)-based optimizers such as spectral gradient descent and Muon are attractive in large-scale learning, but extending them to manifold-constrained problems is nontrivial and often leads to nested-loop schemes that solve tangent-space subproblems iteratively. We propose *Manifold Constrained Steepest Descent* (MCSD), a single-loop framework for optimization over manifolds that selects a norm-induced steepest-descent direction via an LMO applied to the Riemannian gradient, and then returns to the manifold via projection. Under standard smoothness assumptions, we establish convergence guarantees for MCSD and a stochastic momentum variant. We further introduce *SPEL*, the spectral-norm specialization of MCSD on the Stiefel manifold, which admits scalable implementations via fast matrix sign computations. Experiments on PCA, orthogonality-constrained CNNs, and manifold-constrained LLM adapter tuning demonstrate improved stability and competitive performance relative to standard Riemannian baselines and existing manifold-aware LMO methods.

1. Introduction

We study optimization problems over smooth manifolds (1). Such constraints arise throughout computational and applied mathematics, statistics, and machine learning, including linear eigenvalue problems (Liu et al., 2015), k -means clustering (Carson et al., 2017), and batch normalization in deep learning (Cho & Lee, 2017). We refer the readers to Absil et al. (2008); Hu et al. (2020); Boumal (2023) for further background and applications of manifold optimization. A prominent instance is optimization over the *Stiefel manifold* (defined in Section 2.1), which has seen growing use in deep

learning applications. Orthogonality constraints on weight matrices can improve accuracy and speed in CNNs (Bansal et al., 2018) and help reduce overfitting and enhance generalization (Cogswell et al., 2015; Li et al., 2020). They also control conditioning and enable Lipschitz guarantees that are useful for robustness (Anil et al., 2019; Newhouse et al., 2025). In finetuning large language models, Li et al. (2025) extend LoRA (Hu et al., 2022) via a three-factor adapter USV^T with U and V constrained to Stiefel manifolds, and report improvements over several LoRA variants.

Most existing methods for solving the manifold optimization problem can be viewed as Riemannian counterparts of familiar Euclidean optimization methods: one replaces the Euclidean gradient (and, when relevant, Hessian information) with their Riemannian analogues, takes a step in the tangent space, and then uses a retraction (see (3)) to return to the manifold. This perspective yields first-order methods such as Riemannian (stochastic) gradient descent (Bonnabel, 2013), adaptive variants in the spirit of AdaGrad/Adam (Béćigneul & Ganea, 2019; Kasai et al., 2019), and second-order methods including Riemannian Newton and trust-region methods (Absil et al., 2007), with many constructions admitting efficient specializations on the Stiefel manifolds (Li et al., 2020).

In parallel to these Riemannian generalizations of Euclidean optimization methods, there is a line of work on *spectral gradient descent* (SpecGD) for unconstrained Euclidean optimization, where the update direction is obtained by solving a simple linear problem over a spectral-norm ball, equivalently via a matrix linear minimization oracle (LMO) (Carlson et al., 2015; Pethick et al., 2025). Building on this perspective, the recently proposed Muon optimizer (Jordan et al., 2024) has demonstrated strong empirical performance in large language model pretraining (Liu et al., 2025). More broadly, these methods fall under the framework of *Constrained Steepest Descent* (CSD) (Crawshaw et al., 2025), which interprets the update as a steepest-descent step under a chosen norm and thereby offers a flexible way to control relative update magnitudes (Bernstein & Newhouse, 2024).

Given the success of LMO-based methods, a natural question is whether one can obtain *computationally efficient* LMO-based algorithms for manifold-constrained problems, together with convergence guarantees. Recent work has

¹Department of Mathematics, University of Hong Kong, Hong Kong, China. Correspondence to: Lexiao Lai <lai.lexiao@hku.hk>.

begun to explore this direction for Stiefel constraints (Bernstein, 2025; Su, 2025b; Buchanan, 2025; Cesista, 2025). A common approach is to compute a steepest-descent direction by solving an LMO over the *tangent space* subject to a unit-ball constraint under a chosen norm; see (12). In contrast to the unconstrained LMO in the ambient Euclidean space, this tangent-space subproblem generally does not admit a closed-form solution, except in special cases such as the square orthogonal manifold (Su, 2025a). Consequently, existing methods typically rely on iterative inner solvers, including an alternating projection method from Cesista (2025), a dual-based implementation from Su (2025b), the dual subgradient ascent method of Bernstein (2025), and an ADMM-based scheme from Buchanan (2025). The resulting nested-loop structure can be costly at scale, as also reflected in our experiments in Section 5.1. Also, there appears to be no convergence guarantee of these algorithms.

Contributions. We introduce *Manifold Constrained Steepest Descent* (MCSD), a general framework of algorithms for solving manifold optimization problems with *LMO-based* update directions under user-chosen norms, while explicitly enforcing the manifold constraint. MCSD mirrors the simplicity of CSD in Euclidean spaces: each iteration requires evaluating an LMO (often available in closed form) and a projection back to the manifold, yielding a single-loop method with low per-iteration cost when projections are efficient. We also develop stochastic variants of MCSD and establish their convergence guarantees.

As a practically important specialization, we propose *SPEL* (spectral steepest descent on the Stiefel manifold), for optimization problems on Stiefel manifold with the spectral-norm LMO (Table 1). SPEL admits scalable implementations via fast matrix sign computations, leading to Muon-like computational overhead while maintaining Stiefel feasibility at every iterate. We demonstrate SPEL on PCA, orthogonal-constrained convolutional neural networks, and large-language-model adapters, where it improves training stability and is competitive with, or outperforms, standard Riemannian optimization baselines.

Related works. Recent methods have explored norm-constrained optimization in both Euclidean and manifold settings. Pethick et al. (2025) introduce SCG, an LMO-based optimizer over norm balls that unifies and generalizes constrained steepest descent in Euclidean space. Xie et al. (2026) extend this approach with the Spectral Sphere Optimizer (SSO), which constrains both weights and updates to lie on a spectral-norm sphere via a dual-solve step, improving large-scale training stability. Wen et al. (2025) propose Hyperball, a lightweight wrapper that keeps weight norms fixed via Frobenius-norm projection, decoupling step direction from magnitude. Li et al. (2025) develop

StelLA, a manifold-aware optimizer that reparametrizes LoRA adapters as products of SVD factors and applies base optimizers before retracting the gradient back to the tangent space. Relative to these methods, MCSD provides a unified, single-loop framework for norm-constrained optimization over general manifolds, with efficient updates and convergence guarantees.

Organization. The remainder of the paper is organized as follows. Section 2 reviews background on manifold optimization and linear minimization oracles, which will be used to define steepest-descent directions under general norms. Section 3 introduces the proposed Manifold-Constrained Steepest Descent (MCSD) framework and its stochastic variant, and presents SPEL as the spectral-norm specialization on the Stiefel manifold. Section 4 establishes convergence guarantees for MCSD and its stochastic variant under mild regularity conditions, with technical proofs deferred to the appendix. Section 5 evaluates the resulting methods on representative tasks, including PCA, orthogonality-constrained CNN training, and large-scale LLM adapter tuning, and compares against standard Riemannian and LMO-based baselines.

2. Preliminaries

We review basic material on manifold optimization and on linear minimization oracles (LMOs), which together underpin our Manifold constrained Steepest Descent (MCSD) framework.

Notation. Let \mathbb{E} be a Euclidean space with inner product $\langle \cdot, \cdot \rangle$ and induced norm $\|\cdot\|_{\mathbb{E}}$. Given any norm $\|\cdot\|$ on \mathbb{E} , its dual norm $\|\cdot\|_*$ is defined by $\|x\|_* := \sup_{\|d\| \leq 1} \langle d, x \rangle$ for all $x \in \mathbb{E}$. For a set $\mathcal{A} \subset \mathbb{E}$, we denote by $P_{\mathcal{A}}$ the (Euclidean) nearest-point projection,

$$P_{\mathcal{A}}(x) := \arg \min_{y \in \mathcal{A}} \|y - x\|_{\mathbb{E}}, \quad x \in \mathbb{E},$$

which may be set-valued in general. A C^p (*embedded*) manifold $\mathcal{M} \subset \mathbb{E}$ (integer $p \geq 1$) is a subset that locally looks like a p -times continuously differentiable surface: for every $x \in \mathcal{M}$, there exists a neighborhood U of x such that $\mathcal{M} \cap U$ can be parametrized as the image of a C^p map from an open set in \mathbb{R}^m into \mathbb{R}^d . For a point $x \in \mathcal{M}$, we write $T_x \mathcal{M}$ for the tangent space at x . For formal definitions and background on differential geometry, see standard references such as Lee (2012) or Absil et al. (2008).

2.1. Manifold Optimization

We consider the manifold optimization problem (Absil et al., 2008; Hu et al., 2020; Boumal, 2023)

$$\min_{x \in \mathcal{M}} f(x), \quad (1)$$

where $f : \mathbb{E} \rightarrow \mathbb{R}$ is smooth and $\mathcal{M} \subset \mathbb{E}$ is a smooth embedded manifold. For $x \in \mathcal{M}$, the Riemannian gradient of f at x is the orthogonal projection of the Euclidean gradient onto the tangent space (Boumal, 2023, Definition 3.58, Proposition 3.61):

$$\nabla_{\mathcal{M}} f(x) := P_{T_x \mathcal{M}}(\nabla f(x)). \quad (2)$$

A descent step along $-\nabla_{\mathcal{M}} f(x)$ generally leaves the manifold, so manifold optimization methods often combine a tangent-space step with a map back to \mathcal{M} . This is usually done via a *retraction*

$$\text{Retr}_x : T_x \mathcal{M} \rightarrow \mathcal{M}, \quad (3)$$

which locally approximates the Riemannian exponential map and satisfies standard first-order consistency conditions. When the Euclidean projection $P_{\mathcal{M}}$ is single-valued in a neighborhood of x , it induces a natural (projection) retraction, e.g. $\text{Retr}_x(v) := P_{\mathcal{M}}(x + v)$ for sufficiently small v (Absil & Malick, 2012). With a chosen retraction, the classical *Riemannian Gradient Descent (RGD)* update is

$$x_{t+1} = \text{Retr}_{x_t}(-\alpha_t \nabla_{\mathcal{M}} f(x_t)), \quad (4)$$

where $\alpha_t > 0$ is a step size.

The Stiefel manifold. A canonical constraint set considered in manifold optimization problem (1) is the Stiefel manifold, given by

$$\text{St}(n, p) := \{X \in \mathbb{R}^{n \times p} : X^\top X = I_p\},$$

embedded in $\mathbb{R}^{n \times p}$. It reduces to the unit sphere when $p = 1$. For any $X \in \text{St}(n, p)$, its tangent space is

$$T_X \text{St}(n, p) = \{Z \in \mathbb{R}^{n \times p} : X^\top Z + Z^\top X = 0\}. \quad (5)$$

The orthogonal projection of $G \in \mathbb{R}^{n \times p}$ onto $T_X \text{St}(n, p)$ is

$$P_{T_X \text{St}(n, p)}(G) = G - X \text{sym}(X^\top G), \quad (6)$$

where $\text{sym}(A) := \frac{1}{2}(A + A^\top)$. Combining (2) and (6) gives a convenient expression for $\nabla_{\mathcal{M}} f(X)$ when $\mathcal{M} = \text{St}(n, p)$.

Finally, if $Y \in \mathbb{R}^{n \times p}$ has full column rank, its Euclidean projection onto $\text{St}(n, p)$ is the polar factor

$$P_{\text{St}(n, p)}(Y) = Y (Y^\top Y)^{-1/2}.$$

We denote this matrix sign map by

$$\text{msign}(Y) := Y (Y^\top Y)^{-1/2}, \quad (7)$$

noting that given the SVD $Y = U \Sigma V^\top$, one has $\text{msign}(Y) = U V^\top$.

2.2. Linear Minimization Oracle (LMO)

Let $\|\cdot\|$ be a norm on \mathbb{E} . The associated *linear minimization oracle (LMO)* is defined by

$$\text{LMO}_{\|\cdot\|}(s) \in \arg \min_{\|d\| \leq 1} \langle s, d \rangle, \quad s \in \mathbb{E}. \quad (8)$$

By the definition of the dual norm, the optimal value is $-\|s\|_*$; in particular, any choice $d \in \text{LMO}_{\|\cdot\|}(s)$ satisfies $\langle s, d \rangle = -\|s\|_*$. Such oracles arise naturally when constructing steepest-descent directions under a chosen geometry (taking s to be a gradient or gradient-like direction) (Pethick et al., 2025; Crawshaw et al., 2025).

Matrix LMO with the spectral norm. When \mathbb{E} is a matrix space, different matrix norms lead to different closed-form LMOs via (8); see, e.g., Pethick et al. (2025, Tables 2–4). For instance, if $\mathbb{E} = \mathbb{R}^{n \times p}$ and $\|\cdot\|$ is the spectral norm (i.e., the largest singular value of the matrix), then an LMO is given by

$$\text{LMO}_{\|\cdot\|}(S) = -\text{msign}(S), \quad \forall S \in \mathbb{E}.$$

This choice yields the update direction used in spectral gradient descent (Carlson et al., 2015) and, more recently, in the Muon optimizer (Jordan et al., 2024). These algorithms admit cost-effective implementations, thanks to the GPU-friendly iterative schemes for approximating $\text{msign}(\cdot)$, including the classical Newton–Schulz iteration (Schulz, 1933) and recent accelerated variants; see, e.g., Grishina et al. (2025); Amsel et al. (2025).

3. Manifold constrained steepest descent methods

We aim to develop algorithms for the manifold optimization problem (1) that produces iterates on a specified manifold \mathcal{M} . At iteration t , we start from $x_t \in \mathcal{M}$ and assume that the projection $P_{\mathcal{M}}$ onto \mathcal{M} can be computed efficiently. This enables a simple two-step update: take a step in the ambient space along a direction $d_t \in \mathbb{E}$, then project back to \mathcal{M} :

$$x_{t+1} = P_{\mathcal{M}}(x_t + \alpha_t d_t), \quad \forall t \in \mathbb{N}, \quad (9)$$

where $\alpha_t > 0$ is a step size.

It remains to choose the search direction d_t . Since the goal is to decrease f , we select d_t by inspecting the local behavior of the composite map $f \circ P_{\mathcal{M}}$. By Dudek & Holly (1994, Theorem 4.1), the projection mapping $P_{\mathcal{M}}$ is smooth in a neighborhood of \mathcal{M} , and hence $f \circ P_{\mathcal{M}}$ is smooth there as well. Applying a first-order expansion of $f \circ P_{\mathcal{M}}$ at x_t (see

Table 1. One step update of MCSD under different manifolds and norms. We denote by $\|\cdot\|_2$ the spectral norm of matrices. SPEL is short for SPectral gradient descent on the StiefEL manifold.

	$\ \cdot\ = \ \cdot\ _{\mathbb{E}}$	$\ \cdot\ = \ \cdot\ _2$
$\mathcal{M} = \mathbb{R}^{n \times p}$	GD: $x_{t+1} = x_t - \alpha_t \frac{\nabla f(x_t)}{\ \nabla f(x_t)\ _{\mathbb{E}}}$	SpecGD: $x_{t+1} = x_t - \alpha_t \text{msign}(\nabla f(x_t))$
$\mathcal{M} = \text{St}(n, p)$	RGD: $x_{t+1} = \text{msign}\left(x_t - \alpha_t \frac{\nabla_{\mathcal{M}} f(x_t)}{\ \nabla_{\mathcal{M}} f(x_t)\ _{\mathbb{E}}}\right)$	SPEL: $x_{t+1} = \text{msign}(x_t - \alpha_t \text{msign}(\nabla_{\mathcal{M}} f(x_t)))$

Lemma 4.4), we obtain

$$\begin{aligned} f(x_{t+1}) &= f \circ P_{\mathcal{M}}(x_t + \alpha_t d_t) \\ &\leq f(x_t) + \alpha_t \langle \nabla_{\mathcal{M}} f(x_t), d_t \rangle + \frac{L\alpha_t^2}{2} \|d_t\|_{\mathbb{E}}^2. \end{aligned} \quad (10)$$

The appearance of $\nabla_{\mathcal{M}} f(x_t)$ follows from the fact that the differential of $f \circ P_{\mathcal{M}}$ at a point on \mathcal{M} coincides with the Riemannian gradient on the embedded manifold, also by Dudek & Holly (1994, Theorem 4.1).

For sufficiently small α_t , the decrease in f is primarily governed by the linear term $\langle \nabla_{\mathcal{M}} f(x_t), d_t \rangle$. This motivates choosing d_t as a steepest-descent direction with respect to a prescribed norm $\|\cdot\|$, namely as a solution of

$$\min_{\|d\| \leq 1} \langle \nabla_{\mathcal{M}} f(x_t), d \rangle, \quad (11)$$

which is given by the linear minimization oracle

$$d_t = \text{LMO}_{\|\cdot\|}(\nabla_{\mathcal{M}} f(x_t)).$$

This leads to the *manifold constrained steepest descent* (MCSD) method, summarized in Algorithm 1.

Algorithm 1 Manifold Constrained Steepest Descent (MCSD)

Require: Initial point $x_0 \in \mathcal{M}$ and step sizes $(\alpha_t)_{t \in \mathbb{N}}$.

```

1: for  $t = 0, 1, \dots, T-1$  do
2:    $x_{t+1} = P_{\mathcal{M}}(x_t + \alpha_t \text{LMO}_{\|\cdot\|}(\nabla_{\mathcal{M}} f(x_t)))$ 
3: end for
```

Generalizing the constrained steepest descent framework (Crawshaw et al., 2025) (see also (Pethick et al., 2025)), MCSD recovers several standard Euclidean and manifold optimizers under specific choices of \mathcal{M} and $\|\cdot\|$; see Table 1. In particular, when $\mathcal{M} = \text{St}(n, p)$ and $\|\cdot\| = \|\cdot\|_2$, the resulting update yields an optimizer for Stiefel-constrained problems, which we call SPEL. To the best of our knowledge, this specific update rule does not appear in the existing literature. In terms of per-iteration cost, SPEL is only slightly higher than RGD with one additional msign operation. In contrast to RGD and Manifold Muon (Bernstein, 2025), the update direction d_t of SPEL need not lie on the tangent space $T_{x_t} \mathcal{M}$; see Figure 1 for an illustration.

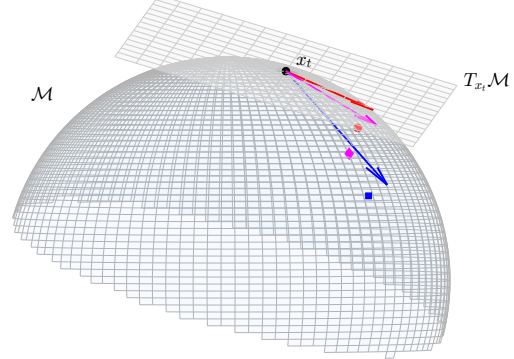


Figure 1. One iteration of Riemannian Gradient Descent, Manifold Muon, and SPEL on the unit sphere.

In large-scale settings, MCSD admits a natural stochastic variant, stated in Algorithm 2. Following common practice in modern optimizers, we incorporate the classical heavy-ball momentum update (Polyak, 1964).

Algorithm 2 Stochastic MCSD

Require: Initial point $x_0 \in \mathcal{M}$, step sizes $(\alpha_t)_{t \in \mathbb{N}}$, and the momentum parameter $\beta \in [0, 1)$.

```

1: for  $t = 0, 1, \dots, T-1$  do
2:   Sample a stochastic gradient  $g_t$  of  $f$  at  $x_t$ 
3:   if  $t > 0$  then
4:      $m_t = \beta m_{t-1} + (1 - \beta) g_t$ 
5:   else
6:      $m_0 = g_0$ 
7:   end if
8:    $x_{t+1} = P_{\mathcal{M}}(x_t + \alpha_t \text{LMO}_{\|\cdot\|}(P_{T_{x_t} \mathcal{M}}(m_t)))$ 
9: end for
```

Remark 3.1 (On efficient implementation of MCSD). For a general manifold \mathcal{M} and a chosen norm $\|\cdot\|$, each iteration of Algorithms 1 and 2 relies on only two primitives: (i) the projection $P_{\mathcal{M}}$ and (ii) a linear minimization oracle $\text{LMO}_{\|\cdot\|}$ with respect to $\|\cdot\|$. Accordingly, MCSD is computationally attractive whenever both operations can be evaluated efficiently. For common norms, the LMO is often available in closed form, reducing to inexpensive coordinate selection or leading singular/eigenvector computations; see, e.g., (Jaggi, 2013; Pethick et al., 2025). Moreover, many

matrix manifolds admit efficient projections: the Stiefel manifold via the msign operation (see (7)), the fixed-rank manifold via truncated SVD (Vandereycken, 2013), and spectral manifolds via eigenvalue projections (Absil & Malick, 2012; Lewis & Malick, 2008). We refer the reader to the aforementioned works for representative applications.

By a slight abuse of terminology, we also refer to the realization of Algorithm 2 with $\mathcal{M} = \text{St}(n, p)$ and $\|\cdot\| = \|\cdot\|_2$ as SPEL.

4. Convergence analysis

In this section, we establish convergence guarantees for MCSD and its stochastic variant under mild regularity conditions. All proofs are deferred to Appendix A. A key technical ingredient—used both to motivate MCSD and to carry out the analysis—is the smoothness of the composition $f \circ P_{\mathcal{M}}$ in a neighborhood of the manifold. We collect the needed properties in the assumption below. For a set $X \subset \mathbb{E}$ and $r > 0$, define $B(X, r) := \cup_{x \in X} B(x, r)$, where $B(x, r) := \{y \in \mathbb{E} : \|x - y\| \leq r\}$ and $\|\cdot\|$ is the norm used in Algorithm 1.

Assumption 4.1. Let $\mathcal{M} \subset \mathbb{E}$ be a C^2 manifold and assume $\inf_{x \in \mathcal{M}} f > -\infty$. Moreover, assume that there exist $r, L > 0$ such that, respect to the Euclidean norm $\|\cdot\|_{\mathbb{E}}$, we have

1. f is differentiable with an L -Lipschitz continuous gradient on \mathcal{M} ;
2. $P_{\mathcal{M}}$ is 2-Lipschitz continuous and C^1 in $B(\mathcal{M}, r)$;
3. For any $\bar{x} \in \mathcal{M}$, $f \circ P_{\mathcal{M}}$ is differentiable with an L -Lipschitz continuous gradient in $B(\bar{x}, r)$.

The first item of the above assumption is standard in manifold optimization; see, e.g., Boumal (2023) or Absil et al. (2008). Items 2 and 3 formalize that the nearest-point projection is well behaved in a tubular neighborhood and that composing with f preserves Lipschitz smoothness locally. These properties are classical consequences of the tubular neighborhood theorem and regularity of the projection map; see, for example, Dudek & Holly (1994) and Lee (2012). The precise statement is stated in the next proposition.

Proposition 4.2. Let $f : \mathbb{E} \rightarrow \mathbb{R}$ be C^1 with a locally Lipschitz gradient and $\mathcal{M} \subset \mathbb{E}$ be a compact C^3 manifold, then Assumption 4.1 holds.

In fact, for the Stiefel manifold one can take an explicit neighborhood size r and give concrete constants in the Lipschitz bound for $\nabla(f \circ P_{\mathcal{M}})$. This relies on regularity of the projection onto $\text{St}(n, p)$ and perturbation bounds for the polar factor.

Proposition 4.3. Let $\mathbb{E} = \mathbb{R}^{n \times p}$ with Frobenius norm $\|\cdot\|_{\mathbb{E}}$, spectral norm $\|\cdot\|$, and let $\mathcal{M} := \text{St}(n, p)$. Assume $f :$

$\mathbb{E} \rightarrow \mathbb{R}$ is C^1 in a neighborhood of \mathcal{M} , and that there exist constants $L_f, G > 0$ such that, for all $u, v \in \mathcal{M}$,

$$\|\nabla f(u) - \nabla f(v)\|_{\mathbb{E}} \leq L_f \|u - v\|_{\mathbb{E}}, \quad \|\nabla f(u)\|_{\mathbb{E}} \leq G.$$

Then Assumption 4.1 holds for \mathcal{M} with

$$r := 0.2, \quad L := 4L_f + 25G.$$

Under Assumption 4.1, we obtain the following upper bound for $f \circ P_{\mathcal{M}}$.

Lemma 4.4. Let Assumption 4.1 hold, then for any $x \in \mathcal{M}$ and $d \in \mathbb{E}$ with $\|d\| \leq r$, we have

$$f \circ P_{\mathcal{M}}(x + d) \leq f(x) + \langle \nabla_{\mathcal{M}} f(x), d \rangle + \frac{L}{2} \|d\|_{\mathbb{E}}^2.$$

We are now ready to prove convergence of MCSD under Assumption 4.1. Given Lemma 4.4, the argument follows the familiar template: apply the inequality with $d = \alpha_t d_t$, telescope the function values, and convert the linear term into a dual-norm decrease. We follow the same style of analysis as in recent work on Muon (Shen et al., 2025), and the resulting complexity bounds align with standard nonconvex first-order guarantees (see, e.g., Bottou et al. (2018); Ghadimi & Lan (2013)). It is worth noticing that when \mathcal{M} is the Stiefel manifold, the step sizes of MCSD can be chosen to be as large as $\Theta(1)$, due to Proposition 4.3.

Theorem 4.5. Let $N > 0$ such that $\|x\|_{\mathbb{E}} \leq N\|x\|$ for all $x \in \mathbb{E}$, where $\|\cdot\|$ is the norm used in Algorithm 1. Under Assumption 4.1, for any realization $(x_t)_{t \in \mathbb{N}}$ of Algorithm 1 with $\alpha_t \in (0, r]$, we have

$$\sum_{t=0}^{T-1} \alpha_t \|\nabla_{\mathcal{M}} f(x_t)\|_* \leq f(x_0) - f(x_T) + \frac{LN^2}{2} \sum_{t=0}^{T-1} \alpha_t^2.$$

Moreover, for any $\Delta \geq f(x_0) - \inf_{x \in \mathcal{M}} f(x)$, if we set $T \geq \frac{2\Delta}{r^2 LN^2}$ and $\alpha_0 = \dots = \alpha_{T-1} = \sqrt{\frac{2\Delta}{T LN^2}}$, then

$$\min_{y=0, \dots, T-1} \|\nabla_{\mathcal{M}} f(x_t)\|_* \leq \sqrt{\frac{2\Delta LN^2}{T}}.$$

Remark 4.6 (On the convergence Manifold Muon). One can also prove the convergence of Manifold Muon on the Stiefel manifold, as described in recent blogs (Su, 2025b; Bernstein, 2025; Cesista, 2025; Buchanan, 2025), using similar arguments as in the proof of Theorem 4.5. Recall that Manifold Muon follows the update (9) with a direction d_t which solves

$$\min_{\|d\| \leq 1, d \in T_{x_t} \mathcal{M}} \langle \nabla_{\mathcal{M}} f(x_t), d \rangle. \quad (12)$$

We have

$$\langle \nabla_{\mathcal{M}} f(x_t), d_t \rangle \leq -\frac{\|\nabla_{\mathcal{M}} f(x_t)\|_{\mathbb{E}}^2}{\|\nabla_{\mathcal{M}} f(x_t)\|} \leq -\frac{N^2}{2} \|\nabla_{\mathcal{M}} f(x_t)\| \quad (13)$$

for some $N > 0$, where the first inequality follows from the fact that $d = -\nabla_{\mathcal{M}} f(x_t)/\|\nabla_{\mathcal{M}} f(x_t)\| \in T_{x_t} \mathcal{M}$ is feasible for (12) and the second inequality is due to the equivalence of norms. Convergence of the manifold Muon follows by plugging (13) into Lemma 4.4, and then applying similar telescoping arguments.

We next prove convergence of stochastic MCSD (Algorithm 2). As is standard in stochastic first-order methods, we assume unbiasedness and bounded variance of the stochastic gradient estimator; see, e.g., Bottou et al. (2018); Robbins & Monro (1951); Ghadimi & Lan (2013).

Assumption 4.7. We assume g_t in Algorithm 2 is an unbiased stochastic estimator of the true gradient $\nabla f(x_t)$ and has a bounded variance, i.e., for some $\sigma > 0$, it holds that

$$\mathbb{E}[g_t] = \nabla f(x_t) \quad \text{and} \quad \mathbb{E}[\|g_t - \nabla f(x_t)\|_{\mathbb{E}}^2] \leq \sigma^2. \quad (14)$$

The convergence guarantee of stochastic MCSD is summarized in the following theorem.

Theorem 4.8. Let $N > 0$ be such that $\|x\|_{\mathbb{E}} \leq N\|x\|$ for all $x \in \mathbb{E}$. Here $\|\cdot\|$ is the norm used in Algorithm 2. Suppose that Assumptions 4.1 and 4.7 hold. Let $(x_t)_{t \in \mathbb{N}}$ be any realization of Algorithm 2 with step sizes $(\alpha_t)_{t \in \mathbb{N}} \subset (0, r]$ and momentum parameter $\beta \in [0, 1)$. For any integer $T \geq 1$, let $\bar{\alpha} := \max_{t=0, \dots, T-1} \alpha_t$. Then

$$\begin{aligned} \sum_{t=0}^{T-1} \alpha_t \mathbb{E}[\|\nabla_{\mathcal{M}} f(x_t)\|_*] &\leq \mathbb{E}[f(x_0) - f(x_T)] \\ &+ 2N \sum_{t=0}^{T-1} \left(\frac{2N\beta L\bar{\alpha}}{1-\beta} + \left(\sqrt{\frac{1-\beta}{1+\beta}} + \beta^t \right) \sigma \right) \alpha_t \\ &+ \frac{LN^2}{2} \sum_{t=0}^{T-1} \alpha_t^2. \end{aligned}$$

Moreover, for any $\Delta \geq f(x_0) - \inf_{x \in \mathcal{M}} f(x)$ and any

$$T \geq \max \left\{ 4, \left(\frac{\Delta}{2LN^2r^2} \right)^{2/3} \right\},$$

if we set

$$\beta := 1 - T^{-1/2}, \quad \alpha_0 = \dots = \alpha_{T-1} := \sqrt{\frac{2\Delta}{LN^2T(8\sqrt{T} - 7)}},$$

then

$$\min_{t=0, \dots, T-1} \mathbb{E}[\|\nabla_{\mathcal{M}} f(x_t)\|_*] \leq 4N(\sqrt{L\Delta} + \sigma)T^{-1/4}.$$

5. Experiments

In this section, we test SPEL on three Stiefel-constrained optimization problems. We begin with a classical PCA

task from manifold optimization literature, then move to orthogonality-constrained convolutional networks to evaluate performance in modern deep learning pipelines, and finally consider large language model fine-tuning to demonstrate the applicability of SPEL in large-scale models. Throughout the experiments, we implement the msign operation using the Polar Express algorithm (Amsel et al., 2025) with eight iterations.

5.1. Principal component analysis (PCA)

Problem. We consider principal component analysis (PCA) with orthogonality constraints (Wold et al., 1987). Given a (centered) data matrix $X \in \mathbb{R}^{n \times d}$ with sample covariance $C := X X^{\top}$, we study the weighted PCA objective

$$\min_{W \in \text{St}(n, p)} f(W) := -\frac{1}{2} \text{tr}(W^{\top} C W D), \quad (15)$$

where $D \in \mathbb{R}^{p \times p}$ is a diagonal matrix with nonnegative entries. When $D = I_p$, the objective is invariant under right-orthogonal transformations and depends only on the subspace $\text{span}(W)$. A non-scalar diagonal D breaks this invariance, induces an ordered orthonormal basis, and yields the Brockett cost, a standard benchmark for optimization on the Stiefel manifold (Brockett, 1991; Edelman et al., 1998; Absil et al., 2008).

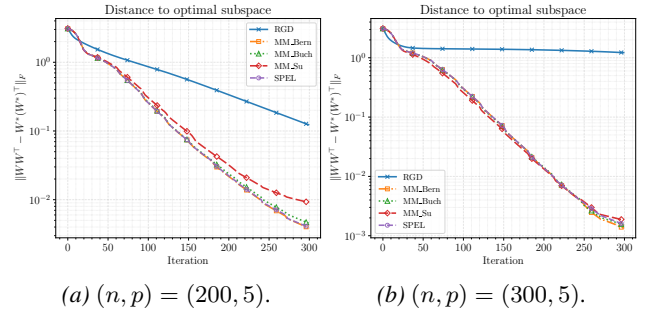


Figure 2. Convergence of manifold optimizers on PCA.

Table 2. Average wall-clock time (in seconds) for solving PCA.

Setting	RGD	MM _{Su}	MM _{Bern}	MM _{Buch}	SPEL
$n = 200$	1.338	11.317	11.108	12.403	2.268
$n = 300$	3.776	32.388	31.331	41.879	6.023

Baselines. We compare SPEL against two representative baselines. (1) *Riemannian gradient descent (RGD)* on the Stiefel manifold, implemented as in Table 1. (2) *Manifold Muon (MM)*, a recent family of LMO-based Stiefel optimizers that (approximately) solve the linear minimization subproblem over tangent spaces in (12) using inner iterative routines. We consider three MM variants that differ only in their inner solvers: a dual-based implementation

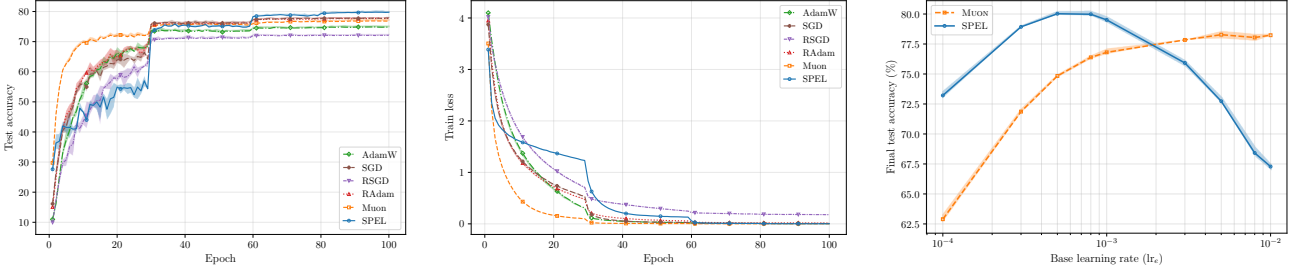


Figure 3. Training Wide ResNet-28 on CIFAR-100. (Left) Test accuracy versus epoch. (Middle) Training loss versus epoch. (Right) Learning-rate sensitivity of SPEL and Muon. Curves are averaged over 3 runs; shaded regions indicate run-to-run variability.

from Su (2025b) (MM_{Su}¹), the dual subgradient ascent of Bernstein (2025) (MM_{Bern}²), and an ADMM-based scheme from Buchanan (2025) (MM_{Buch}³).

Implementation details. We set $p = 5$, $d = 1000$, and generate $X \in \mathbb{R}^{n \times d}$ with entries following standard normal distributions. All methods are initialized from the same point on $\text{St}(n, p)$. For MM variants, we cap the number of inner iterations at 10. We adopt the same setting for all other hyperparameters as the original implementations. We report results for $n \in \{200, 300\}$, running each method for $T = 300$ iterations on a MacBook Pro (M1 Max).

RGD uses a constant step size $\alpha_t = 10^{-3}$ selected by grid search; a step-size sensitivity study is provided in Figure 4 (appendix B.1). SPEL and all MM variants use a periodically decayed schedule $\alpha_t = 0.1 \cdot 0.5^{\lfloor t/30 \rfloor}$. Performance is measured by the Frobenius subspace error $\|W_t W_t^\top - W^* W^{*\top}\|_F$, where $W^* \in \text{St}(n, p)$ is computed by applying SVD to the covariance matrix.

Results. Figure 2 and Table 2 summarize the results. As a function of iteration count, SPEL achieves comparable accuracy to all MM variants and consistently outperforms RGD, with the gap widening as n increases. In wall-clock time, SPEL is substantially faster than MM because it is single-loop and avoids solving subproblems at each iteration (Table 2).

5.2. Orthogonality in CNNs

Problem. We consider the problem of training convolutional neural networks (CNNs) under orthogonality constraints, as discussed by Li et al. (2020). Specifically, each convolutional kernel $K \in \mathbb{R}^{c_{\text{out}} \times c_{\text{in}} \times k \times h}$ is reshaped into a matrix of size $p \times n = c_{\text{out}} \times (c_{\text{in}} \cdot k \cdot h)$, and is constrained on the Stiefel manifold. We evaluate Euclidean and

Table 3. Training Wide ResNet-28 on CIFAR-100 with results averaged over 3 runs. Train Time reflects the average epoch time.

Optimizer	Test Acc. (%)	Train Loss	Train Time (s)
SGD	77.92	0.0089	30.99
AdamW	74.78	0.0051	31.09
Muon	76.81	0.0009	34.29
RSGD	72.14	0.1788	34.94
RAdam	77.68	0.0162	35.24
SPEL	79.75	0.0016	40.24

manifold optimizers on the CIFAR-100 classification task (Krizhevsky et al., 2009) using Wide ResNet-28 (Zagoruyko & Komodakis, 2016).

Baselines. We compare SPEL against two groups of baselines. *Euclidean optimizers* (SGD, AdamW (Loshchilov & Hutter, 2019), and Muon (Jordan et al., 2024)) train the network without enforcing any orthogonality constraints. Since Muon is defined only for matrix parameters, we apply it to the convolutional and fully connected layers, and optimize the remaining parameters with AdamW.

We also evaluate other *manifold optimizers* that explicitly enforce Stiefel constraints. Specifically, we implement Riemannian SGD (RSGD) and Riemannian Adam (RAdam) following Li et al. (2020), using retractions induced by the msign operator. An ablation on the choice of retraction is deferred to Table 5 in the appendix. The manifold optimizers are applied only to the convolutional layers with Stiefel constraints; the remaining parameters are updated in the Euclidean space. Following Li et al. (2020), we use SGD to update the unconstrained weights for both RSGD and RAdam. For SPEL, we mirror the Muon implementation: AdamW is applied to bias parameters, while Muon is used for fully connected layers.

Implementation details. We follow the implementation⁴

¹<https://kexue.fm/archives/11221>

²<https://github.com/thinking-machines-lab/manifolds/>

³<https://sdbuchanan.com/blog/manifold-muon/>

⁴<https://github.com/JunLi-Galios/Optimization-on-Stiefel-Manifold-via-Cayley-Transform>

Manifold constrained steepest descent

Table 4. Accuracy (in %) on the commonsense reasoning benchmark with LLaMA models. Results are averaged over three runs.

Model	Optimizer	BoolQ	PIQA	SIQA	HellaS.	WinoG.	ARC-e	ARC-c	OBQA	Avg.
LLaMA-3-8B	SPEL	76.25	89.14	81.70	96.18	87.32	91.82	81.80	87.67	86.49
	StellA	76.23	89.44	81.68	96.44	88.27	92.49	82.17	87.20	86.74
LLaMA-3.1-8B	SPEL	76.24	89.94	81.29	96.25	87.03	91.87	81.20	88.00	86.48
	StellA	76.10	89.50	81.41	96.44	87.63	91.93	82.03	87.33	86.55

and hyperparameter choices of [Li et al. \(2020\)](#). For Euclidean baselines, we use base learning rates 0.1 for SGD and 10^{-3} for AdamW. For Muon, we set the base learning rate to 10^{-3} and apply the layerwise scaling rule of [Liu et al. \(2025, Equation \(4\)\)](#): for each matrix parameter of size $p \times n$, the learning rate is multiplied by $0.2\sqrt{\max(p, n)}$. This scaling rule is known to enable reliable learning-rate transfer when switching from AdamW to Muon.

For manifold optimizers, we use separate learning rates for different parameter groups: lr_s for Stiefel-constrained parameters and lr_e for unconstrained parameters. We set $(lr_s, lr_e) = (0.2, 0.01)$ for RSGD and $(lr_s, lr_e) = (0.4, 0.01)$ for RAdam. For SPEL, we use $(lr_s, lr_e) = (0.003, 0.001)$ and apply the same layerwise scaling factor $0.2\sqrt{\max\{p, n\}}$ as in Muon to both lr_s and lr_e ; we find that SPEL is relatively insensitive to lr_s over a reasonable range (Figure 6 in appendix). Across all methods, we decay the learning rate by a factor of 0.2 at epochs 30, 60, and 80. All experiments are run on a single NVIDIA A100 GPU.

Results. Table 3 and Figure 3 summarize the training and test performance. Overall, SPEL attains the best final test accuracy while keeping training time competitive. Muon decreases the training loss rapidly (Figure 3, middle), but its final test accuracy is lower than that of SGD, RAdam, and SPEL.

To assess learning-rate sensitivity, we sweep the base learning rate for SPEL and Muon (Figure 3, right). For SPEL, we fix the ratio between the learning rates of constrained and unconstrained parameters to $lr_s/lr_e = 3$, guided by the robustness region in Figure 6 (appendix B.2), and vary lr_e to mirror the sweep protocol used for Muon. Both methods are stable over a broad range of learning rates; moreover, when the learning rate is well tuned, SPEL consistently achieves higher accuracy than Muon.

5.3. LLM adapter tuning: StellA with SPEL

Problem. We evaluate SPEL on large-scale language model adaptation through StellA (Stiefel Low-Rank Adaptation) ([Li et al., 2025](#)), a recently proposed orthogonality-constrained adapter that improves over standard LoRA variants. StellA can be viewed as a manifold-constrained analogue of LoRA, where a subset of adapter factors are con-

strained to lie on the Stiefel manifold. We consider the commonsense reasoning benchmark used in prior adapter studies ([Hu et al., 2023; Liu et al., 2024](#)), which comprises eight sub-tasks. Following [Li et al. \(2025\)](#), we train on the union of the training sets from all sub-tasks and report test performance. We finetune two widely used checkpoints, LLaMA-3-8B ([Dubey et al., 2024](#)) and LLaMA-3.1-8B ([Vavekanand & Sam, 2024](#)).

Baseline and implementation. We compare against the optimizer used in StellA ([Li et al., 2025](#)), which wraps AdamW with a Stiefel-aware update for constrained parameters; this is referred to as StellA in Table 4. In our implementation, SPEL is applied to the Stiefel-constrained adapter parameters, while the remaining (unconstrained) parameters are updated by the same AdamW configuration. We use the official adapter codebase⁵ and match the experimental setup of [Li et al. \(2025\)](#). For both SPEL and the StellA optimizer, we use a base learning rate of 5×10^{-4} with linear decay and a 500-step warm-up. In addition, SPEL uses the same layerwise learning-rate scaling rule as in [Liu et al. \(2025\)](#), consistent with our CNN experiments. All experiments are run on a single NVIDIA H100 GPU.

Results. Table 4 reports accuracy on the eight downstream tasks for commonsense reasoning. Across both LLaMA checkpoints, SPEL matches the StellA optimizer in final accuracy and exhibits similar training dynamics (Figure 7 in appendix). SPEL also reduces optimizer state memory, since it does not store second-moment estimates. These results show that SPEL is a drop-in optimizer for Stiefel-constrained adapter tuning at LLM scale: under the same training setup as StellA and without additional tuning, it matches the downstream accuracy and training dynamics of the StellA optimizer while using a lighter optimizer state.

Acknowledgements

This work is partially supported by a start-up fund at the University of Hong Kong and by the Hong Kong Research Grants Council under ECS project 27301425. A part of the computations were performed using research computing facilities offered by Information Technology Services, the

⁵<https://github.com/SonyResearch/stella>

University of Hong Kong.

Impact Statement

This paper presents work whose goal is to advance the field of Machine Learning. There are many potential societal consequences of our work, none which we feel must be specifically highlighted here.

References

Absil, P.-A. and Malick, J. Projection-like retractions on matrix manifolds. *SIAM Journal on Optimization*, 22(1): 135–158, 2012.

Absil, P.-A., Baker, C. G., and Gallivan, K. A. Trust-region methods on riemannian manifolds. *Foundations of Computational Mathematics*, 7(3):303–330, 2007.

Absil, P.-A., Mahony, R., and Sepulchre, R. *Optimization algorithms on matrix manifolds*. Princeton University Press, 2008.

Amsel, N., Persson, D., Musco, C., and Gower, R. M. The polar express: Optimal matrix sign methods and their application to the muon algorithm. *arXiv preprint arXiv:2505.16932*, 2025.

Anil, C., Lucas, J., and Grosse, R. Sorting out lipschitz function approximation. In *International conference on machine learning*, pp. 291–301. PMLR, 2019.

Bansal, N., Chen, X., and Wang, Z. Can we gain more from orthogonality regularizations in training deep networks? *Advances in Neural Information Processing Systems*, 31, 2018.

Bécigneul, G. and Ganea, O. Riemannian adaptive optimization methods. In *Proceedings of the 7th International Conference on Learning Representations (ICLR)*, May 6-9 2019.

Bernstein, J. Modular manifolds. *Thinking Machines Lab: Connectionism*, 2025. doi: 10.64434/tml.20250926. URL <https://thinkingmachines.ai/blog/modular-manifolds/>.

Bernstein, J. and Newhouse, L. Old optimizer, new norm: An anthology. In *Proceedings of OPT 2024: Optimization for Machine Learning*, 2024.

Bonnabel, S. Stochastic gradient descent on riemannian manifolds. *IEEE Transactions on Automatic Control*, 58(9):2217–2229, 2013.

Bottou, L., Curtis, F. E., and Nocedal, J. Optimization methods for large-scale machine learning. *Siam Review*, 60(2):223–311, 2018.

Boumal, N. *An introduction to optimization on smooth manifolds*. Cambridge University Press, 2023.

Brockett, R. W. Dynamical systems that sort lists, diagonalize matrices, and solve linear programming problems. *Linear Algebra and its applications*, 146:79–91, 1991.

Buchanan, S. A faster manifold muon with ADMM, 2025. URL <https://sdbuchanan.com/blog/manifold-muon/>.

Carlson, D. E., Collins, E., Hsieh, Y.-P., Carin, L., and Cevher, V. Preconditioned spectral descent for deep learning. *Advances in neural information processing systems*, 28, 2015.

Carson, T., Mixon, D. G., Villar, S., and Ward, R. Manifold optimization for k-means clustering. In *2017 International Conference on Sampling Theory and Applications (SampTA)*, pp. 73–77. IEEE, 2017.

Cesista, F. L. Heuristic solutions for Steepest Descent on the Stiefel manifold, July 2025. URL <https://leloykun.github.io/ponder/steepest-descent-stiefel/>.

Cho, M. and Lee, J. Riemannian approach to batch normalization. *Advances in Neural Information Processing Systems*, 30, 2017.

Clarke, F. H., Stern, R. J., and Wolenski, P. R. Proximal smoothness and the lower-c2 property. *J. Convex Anal.*, 2(1-2):117–144, 1995.

Cogswell, M., Ahmed, F., Girshick, R., Zitnick, L., and Batra, D. Reducing overfitting in deep networks by decorrelating representations. *arXiv preprint arXiv:1511.06068*, 2015.

Crawshaw, M., Modi, C., Liu, M., and Gower, R. M. An exploration of non-euclidean gradient descent: Muon and its many variants. *arXiv preprint arXiv:2510.09827*, 2025.

Dubey, A., Jauhri, A., Pandey, A., Kadian, A., Al-Dahle, A., Letman, A., Mathur, A., Schelten, A., Yang, A., Fan, A., et al. The llama 3 herd of models. *arXiv e-prints*, pp. arXiv–2407, 2024.

Dudek, E. and Holly, K. Nonlinear orthogonal projection. In *Annales Polonici Mathematici*, volume 59, pp. 1–31. Polska Akademia Nauk. Instytut Matematyczny PAN, 1994.

Edelman, A., Arias, T. A., and Smith, S. T. The geometry of algorithms with orthogonality constraints. *SIAM journal on Matrix Analysis and Applications*, 20(2):303–353, 1998.

Federer, H. Curvature measures. *Transactions of the American Mathematical Society*, 93(3):418–491, 1959.

Ghadimi, S. and Lan, G. Stochastic first-and zeroth-order methods for nonconvex stochastic programming. *SIAM journal on optimization*, 23(4):2341–2368, 2013.

Grishina, E., Smirnov, M., and Rakhuba, M. Accelerating newton-schulz iteration for orthogonalization via chebyshev-type polynomials. *arXiv preprint arXiv:2506.10935*, 2025.

Hu, E. J., Shen, Y., Wallis, P., Allen-Zhu, Z., Li, Y., Wang, S., Wang, L., and Chen, W. Lora: Low-rank adaptation of large language models. In *Proceedings of the Tenth International Conference on Learning Representations (ICLR)*, Virtual Event, April 25–29 2022.

Hu, J., Liu, X., Wen, Z.-W., and Yuan, Y.-X. A brief introduction to manifold optimization. *Journal of the Operations Research Society of China*, 8(2):199–248, 2020.

Hu, Z., Wang, L., Lan, Y., Xu, W., Lim, E.-P., Bing, L., Xu, X., Poria, S., and Lee, R. Llm-adapters: An adapter family for parameter-efficient fine-tuning of large language models. In *Proceedings of the 2023 conference on empirical methods in natural language processing*, pp. 5254–5276, 2023.

Jaggi, M. Revisiting frank-wolfe: Projection-free sparse convex optimization. In *International conference on machine learning*, pp. 427–435. PMLR, 2013.

Jordan, K., Jin, Y., Boza, V., Jiacheng, Y., Cesista, F., Newhouse, L., and Bernstein, J. Muon: An optimizer for hidden layers in neural networks, 2024. URL <https://kellerjordan.github.io/posts/muon/>.

Kasai, H., Jawanpuria, P., and Mishra, B. Riemannian adaptive stochastic gradient algorithms on matrix manifolds. In *International conference on machine learning*, pp. 3262–3271. PMLR, 2019.

Krizhevsky, A., Hinton, G., et al. Learning multiple layers of features from tiny images. 2009.

Lee, J. M. *Introduction to Smooth Manifolds*. Springer New York, NY, 2012.

Lewis, A. S. and Malick, J. Alternating projections on manifolds. *Mathematics of Operations Research*, 33(1): 216–234, 2008.

Li, J., Li, F., and Todorovic, S. Efficient riemannian optimization on the stiefel manifold via the cayley transform. In *Proceedings of the 8th International Conference on Learning Representations (ICLR)*, April 26–30 2020.

Li, Z., Sajadmanesh, S., Li, J., and Lyu, L. Stella: Subspace learning in low-rank adaptation using stiefel manifold. In *Advances in Neural Information Processing Systems*, 2025.

Liu, J., Su, J., Yao, X., Jiang, Z., Lai, G., Du, Y., Qin, Y., Xu, W., Lu, E., Yan, J., et al. Muon is scalable for llm training. *arXiv preprint arXiv:2502.16982*, 2025.

Liu, S.-Y., Wang, C.-Y., Yin, H., Molchanov, P., Wang, Y.-C. F., Cheng, K.-T., and Chen, M.-H. Dora: Weight-decomposed low-rank adaptation. In *Forty-first International Conference on Machine Learning*, 2024.

Liu, X., Wen, Z., and Zhang, Y. An efficient gauss–newton algorithm for symmetric low-rank product matrix approximations. *SIAM Journal on Optimization*, 25(3):1571–1608, 2015.

Loshchilov, I. and Hutter, F. Decoupled weight decay regularization. In *Proceedings of the 7th International Conference on Learning Representations (ICLR)*, 2019.

Newhouse, L., Hess, R. P., Cesista, F., Zahorodnii, A., Bernstein, J., and Isola, P. Training transformers with enforced lipschitz constants. *arXiv preprint arXiv:2507.13338*, 2025.

Pethick, T., Xie, W., Antonakopoulos, K., Zhu, Z., Silveti-Falls, A., and Cevher, V. Training deep learning models with norm-constrained lmos. In *Proceedings of the Forty-Second International Conference on Machine Learning (ICML)*, July 13–19 2025.

Polyak, B. T. Some methods of speeding up the convergence of iteration methods. *USSR Computational Mathematics and Mathematical Physics*, 4(5):1–17, 1964.

Robbins, H. and Monro, S. A stochastic approximation method. *The annals of mathematical statistics*, pp. 400–407, 1951.

Schulz, G. Iterative berechung der reziproken matrix. *ZAMM-Journal of Applied Mathematics and Mechanics/Zeitschrift für Angewandte Mathematik und Mechanik*, 13(1):57–59, 1933.

Shen, W., Huang, R., Huang, M., Shen, C., and Zhang, J. On the convergence analysis of muon. *arXiv preprint arXiv:2505.23737*, 2025.

Su, J. Steepest desecent on manifolds: 2. muon + orthogonality, Aug 2025a. URL <https://kexue.fm/archives/11215>.

Su, J. Steepest desecent on manifolds: 3. muon + stiefel, Aug 2025b. URL <https://kexue.fm/archives/11221>.

Vandereycken, B. Low-rank matrix completion by riemannian optimization. *SIAM Journal on Optimization*, 23(2):1214–1236, 2013.

Vavekanand, R. and Sam, K. Llama 3.1: An in-depth analysis of the next-generation large language model. *Preprint, July*, 2024.

Wen, K., Dang, X., Lyu, K., Ma, T., and Liang, P. Fantastic pretraining optimizers and where to find them 2.1: Hyperball optimization, 12 2025. URL <https://tinyurl.com/muonh>.

Wold, S., Esbensen, K., and Geladi, P. Principal component analysis. *Chemometrics and intelligent laboratory systems*, 2(1-3):37–52, 1987.

Xie, T., Luo, H., Tang, H., Hu, Y., Liu, J. K., Ren, Q., Wang, Y., Zhao, W. X., Yan, R., Su, B., et al. Controlled llm training on spectral sphere. *arXiv preprint arXiv:2601.08393*, 2026.

Zagoruyko, S. and Komodakis, N. Wide residual networks. In Wilson, R. C., Hancock, E. R., and Smith, W. A. P. (eds.), *Proceedings of the British Machine Vision Conference 2016 (BMVC)*, York, UK, September 19-22 2016. BMVA Press.

Appendix

A	Convergence analysis of MCSD	13
A.1	Proof of Proposition 4.2	13
A.2	Proof of Proposition 4.3	14
A.3	Proof of Lemma 4.4	17
A.4	Proof of Theorem 4.5	17
A.5	Proof of Theorem 4.8	18
B	Supplementary experimental results	21
B.1	Principal component analysis (PCA)	21
B.2	Orthogonality in CNNs	22
B.3	LLM adapter tuning: StelLA with SPEL	23

A. Convergence analysis of MCSD

A.1. Proof of Proposition 4.2

We recall below some known facts for the projection onto smooth manifolds from (Dudek & Holly, 1994).

Theorem A.1. (Dudek & Holly, 1994, Section 4) *Let $k \geq 2$ and $\mathcal{M} \subset \mathbb{E}$ be a C^k manifold, then there exists a neighborhood Ω of \mathcal{M} such that*

1. $P_{\mathcal{M}}$ is single-valued and is C^{k-1} in Ω and;
2. $DP_{\mathcal{M}}(x) = P_{T_x \mathcal{M}}$ for any $x \in \mathcal{M}$.

In the context of the theorem above, fix any $x \in \mathbb{E}$, the Jacobian $DP_{\mathcal{M}}(x) : \mathbb{E} \rightarrow \mathbb{E}$ is a linear map and the second-order derivative $D^2P_{\mathcal{M}}(x) : \mathbb{E} \times \mathbb{E} \rightarrow \mathbb{E}$ is a bilinear map. Recall that their operator norms, with respect to the Euclidean norm $\|\cdot\|_{\mathbb{E}}$, are defined respectively as follows:

$$\|DP_{\mathcal{M}}(x)\|_{\text{op}} := \sup_{y \neq 0} \frac{\|DP_{\mathcal{M}}(x)[y]\|_{\mathbb{E}}}{\|y\|_{\mathbb{E}}} \quad \text{and} \quad \|D^2P_{\mathcal{M}}(x)\|_{\text{op}} := \sup_{y, z \neq 0} \frac{\|D^2P_{\mathcal{M}}(x)[y, z]\|_{\mathbb{E}}}{\|y\|_{\mathbb{E}}\|z\|_{\mathbb{E}}}.$$

Assuming that P is C^2 along a line segment $[x, y] \subset \Omega$, then by the fundamental theorem of calculus, we have

$$\|DP_{\mathcal{M}}(x) - DP_{\mathcal{M}}(y)\|_{\text{op}} \leq \sup_{z \in [x, y]} \|D^2P_{\mathcal{M}}(z)\|_{\text{op}} \|x - y\|_{\mathbb{E}}.$$

In the following lemma, we provide a uniform upper bound on $\|D^2P_{\mathcal{M}}(x)\|_{\text{op}}$ near the manifold \mathcal{M} , in order to establish the Lipschitz continuity of $DP_{\mathcal{M}}$.

Lemma A.2. *Let $M \subset \mathbb{E}$ be a C^3 manifold and let $X \subset M$ be a compact. Then there exist $r, B > 0$ such that $P_{\mathcal{M}}$ is C^2 in $B(X, r)$ and we have $\|D^2P_{\mathcal{M}}(x)\|_{\text{op}} \leq B$ for any $x \in B(X, r)$.*

Proof. Since \mathcal{M} is a C^3 manifold in \mathbb{E} , Theorem A.1 implies that $P_{\mathcal{M}}$ is C^2 in some open neighborhood Ω of \mathcal{M} . As X is compact, there exists $r > 0$ such that $B(X, r) \subset \Omega$. Since $B(X, r)$ is compact and the mapping $x \mapsto \|D^2P_{\mathcal{M}}(x)\|_{\text{op}}$ is continuous on Ω , it holds that $\infty > \sup_{x \in B(X, r)} \|D^2P_{\mathcal{M}}(x)\|_{\text{op}} =: B$. \square

We are now ready to prove Proposition 4.2.

Proof of Proposition 4.2. Since \mathcal{M} is a compact C^3 manifold and $f : \mathbb{E} \rightarrow \mathbb{R}$ is continuous, $\inf_{x \in \mathcal{M}} f > -\infty$. As f is also C^1 with a locally Lipschitz gradient, there exist $L, G > 0$ such that

$$\|\nabla f(x) - \nabla f(y)\|_{\mathbb{E}} \leq L \|x - y\|_{\mathbb{E}}, \quad \|\nabla f(x)\|_{\mathbb{E}} \leq G \quad (16)$$

for all $x, y \in M$. By Lemma A.2, there exist $r, B > 0$ such that $P_{\mathcal{M}}$ is C^2 in $B(\mathcal{M}, 2r)$ and we have $\|D^2P_{\mathcal{M}}(x)\|_{\text{op}} \leq B$ for any $x \in B(\mathcal{M}, 2r)$. According to (Federer, 1959, 4.8 Theorem) (or, see (Clarke et al., 1995, Theorem 4.8)), $P_{\mathcal{M}}$ is 2-Lipschitz in $B(\mathcal{M}, r)$. It follows that $\|DP_{\mathcal{M}}(x)\|_{\text{op}} \leq 2$ for all $x \in B(\mathcal{M}, r)$.

Lastly, we derive the Lipschitz continuity of $\nabla(f \circ P_{\mathcal{M}})$. By chain rule, it holds that $f \circ P_{\mathcal{M}}$ is C^1 in $B(\mathcal{M}, r)$. Fix any $\bar{x} \in M$, for any $x, x' \in B(\bar{x}, r)$, we have

$$\begin{aligned} & \|\nabla(f \circ P_{\mathcal{M}})(x) - \nabla(f \circ P_{\mathcal{M}})(x')\|_{\mathbb{E}} \\ &= \|DP_{\mathcal{M}}(x)\nabla f(P_{\mathcal{M}}(x)) - DP_{\mathcal{M}}(x')\nabla f(P_{\mathcal{M}}(x'))\|_{\mathbb{E}} \\ &\leq \|DP_{\mathcal{M}}(x)(\nabla f(P_{\mathcal{M}}(x)) - \nabla f(P_{\mathcal{M}}(x')))\|_{\mathbb{E}} + \|(DP_{\mathcal{M}}(x) - DP_{\mathcal{M}}(x'))\nabla f(P_{\mathcal{M}}(x'))\|_{\mathbb{E}} \quad (17) \\ &\leq \|DP_{\mathcal{M}}(x)\|_{\text{op}} \|\nabla f(P_{\mathcal{M}}(x)) - \nabla f(P_{\mathcal{M}}(x'))\|_{\mathbb{E}} + \|DP_{\mathcal{M}}(x) - DP_{\mathcal{M}}(x')\|_{\text{op}} \|\nabla f(P_{\mathcal{M}}(x'))\|_{\mathbb{E}} \\ &\leq 4L\|x - x'\|_{\mathbb{E}} + B\|x - x'\|_{\mathbb{E}} \times G, \end{aligned}$$

where we used Theorem A.1 and the convexity of $B(\bar{x}, r)$. Thus, Assumption 4.1 holds after increasing L . \square

A.2. Proof of Proposition 4.3

Lemma A.3 (Stiefel-specific bound on $D^2P_{\mathcal{M}}$ in a tubular neighborhood). *Let $\mathbb{E} = \mathbb{R}^{n \times p}$ with Frobenius norm $\|\cdot\|_F$, and*

$$M := \text{St}(n, p) := \{X \in \mathbb{R}^{n \times p} : X^\top X = I_p\}.$$

Let $P_{\mathcal{M}}$ be the Euclidean projection onto \mathcal{M} . For $r \in (0, 1)$ define

$$B(r) := \sup_{Y \in B(\mathcal{M}, r)} \|D^2P_{\mathcal{M}}(Y)\|_{\text{op}}.$$

Then for every $r \in (0, 1)$,

$$B(r) \leq C(r) := 3 \frac{1+r}{(1-r)^3} + 3 \frac{(1+r)^3}{(1-r)^5}.$$

In particular, for $r = \frac{1}{5}$,

$$B\left(\frac{1}{5}\right) \leq \frac{2925}{128} < 25,$$

so on $B(M, \frac{1}{5})$ one may take $B_ := 25$ as a uniform upper bound for $\|D^2P_{\mathcal{M}}(Y)\|_{\text{op}}$.*

Proof. We use the Frobenius norm on all matrix spaces and the associated operator norm on multilinear maps.

1. Basic maps and their derivatives. Define

$$A(Y) := Y^\top Y \in \mathbb{R}^{p \times p}, \quad f(A) := A^{-1/2}, \quad P_{\mathcal{M}}(Y) := Yf(A(Y)).$$

(a) *Derivatives of $A(Y)$.* For $H, K \in \mathbb{R}^{n \times p}$,

$$A(Y + H) = (Y + H)^\top (Y + H) = Y^\top Y + H^\top Y + Y^\top H + H^\top H,$$

so

$$DA(Y)[H] = H^\top Y + Y^\top H, \quad D^2A(Y)[H, K] = H^\top K + K^\top H.$$

(b) *Derivatives of $f(A) = A^{-1/2}$.* For scalars $\lambda > 0$ one has

$$\lambda^{-1/2} = \frac{1}{\pi} \int_0^\infty \frac{t^{-1/2}}{\lambda + t} dt,$$

hence for SPD A ,

$$A^{-1/2} = \frac{1}{\pi} \int_0^\infty t^{-1/2} (A + tI)^{-1} dt$$

(via spectral calculus). Differentiating under the integral sign gives, for symmetric E, F ,

$$Df(A)[E] = -\frac{1}{\pi} \int_0^\infty t^{-1/2} (A + tI)^{-1} E (A + tI)^{-1} dt,$$

$$D^2f(A)[E, F] = \frac{1}{\pi} \int_0^\infty t^{-1/2} \left[(A + tI)^{-1} E (A + tI)^{-1} F (A + tI)^{-1} + (A + tI)^{-1} F (A + tI)^{-1} E (A + tI)^{-1} \right] dt.$$

Let $m := \lambda_{\min}(A) > 0$. Then $A + tI \succeq (m + t)I$ and

$$\|(A + tI)^{-1}\|_2 \leq \frac{1}{m + t}.$$

Hence

$$\|Df(A)[E]\|_2 \leq \frac{1}{\pi} \int_0^\infty t^{-1/2} \frac{1}{(m + t)^2} dt \|E\|_2,$$

$$\|D^2 f(A)[E, F]\|_2 \leq \frac{2}{\pi} \int_0^\infty t^{-1/2} \frac{1}{(m+t)^3} dt \|E\|_2 \|F\|_2.$$

The integrals are elementary:

$$\begin{aligned} \int_0^\infty \frac{t^{-1/2}}{(m+t)^2} dt &= m^{-3/2} \int_0^\infty \frac{u^{-1/2}}{(1+u)^2} du = m^{-3/2} \cdot \frac{\pi}{2}, \\ \int_0^\infty \frac{t^{-1/2}}{(m+t)^3} dt &= m^{-5/2} \int_0^\infty \frac{u^{-1/2}}{(1+u)^3} du = m^{-5/2} \cdot \frac{3\pi}{8}. \end{aligned}$$

Thus

$$\|Df(A)\|_{\text{op}} \leq \frac{1}{2} m^{-3/2}, \quad \|D^2 f(A)\|_{\text{op}} \leq \frac{3}{4} m^{-5/2}.$$

In our setting $A = Y^\top Y$ has eigenvalues $\sigma_i(Y)^2$, so

$$m = \lambda_{\min}(A) = \sigma_{\min}(Y)^2, \quad \|Df(A)\|_{\text{op}} \leq \frac{1}{2} \sigma_{\min}(Y)^{-3}, \quad \|D^2 f(A)\|_{\text{op}} \leq \frac{3}{4} \sigma_{\min}(Y)^{-5}.$$

2. First and second derivatives of $P_{\mathcal{M}}$. Write $A = A(Y)$ for brevity and define

$$\begin{aligned} E_H &:= DA(Y)[H] = H^\top Y + Y^\top H, & E_K &:= DA(Y)[K] = K^\top Y + Y^\top K, \\ G(H, K) &:= D^2 A(Y)[H, K] = H^\top K + K^\top H. \end{aligned}$$

(a) *First derivative.* For $P_{\mathcal{M}}(Y) = Y f(A(Y))$, the chain rule gives

$$DP_{\mathcal{M}}(Y)[H] = H f(A) + Y Df(A)[E_H].$$

(b) *Second derivative.* Differentiate $DP_{\mathcal{M}}(Y)[H]$ with respect to Y in direction K . The first term gives

$$D(H f(A(Y)))[K] = H Df(A)[E_K].$$

For the second term, write $\Phi(Y) := Df(A(Y))[E_H(Y)]$. Then

$$D(Y \Phi(Y))[K] = K \Phi(Y) + Y D\Phi(Y)[K].$$

By the second-order chain rule,

$$D\Phi(Y)[K] = D^2 f(A)[E_K, E_H] + Df(A)[G(H, K)].$$

Therefore

$$D^2 P_{\mathcal{M}}(Y)[H, K] = H Df(A)[E_K] + K Df(A)[E_H] + Y D^2 f(A)[E_K, E_H] + Y Df(A)[G(H, K)].$$

3. Norm bounds. We now bound $\|D^2 P_{\mathcal{M}}(Y)[H, K]\|_F$ in terms of $\|H\|_F \|K\|_F$ and the singular values of Y .

Let $\sigma_{\min} := \sigma_{\min}(Y)$ and $\sigma_{\max} := \sigma_{\max}(Y)$. Then

$$\begin{aligned} \|Y\|_2 &= \sigma_{\max}, & \|E_H\|_F &\leq \|H^\top Y\|_F + \|Y^\top H\|_F \leq 2\sigma_{\max}\|H\|_F, \\ \|E_K\|_F &\leq 2\sigma_{\max}\|K\|_F, & \|G(H, K)\|_F &\leq 2\|H\|_F\|K\|_F. \end{aligned}$$

Using the bounds on Df and $D^2 f$ and the inequality $\|AB\|_F \leq \|A\|_2 \|B\|_F$:

Term 1: $T_1 := H Df(A)[E_K]$.

$$\|T_1\|_F \leq \|H\|_F \|Df(A)\|_{\text{op}} \|E_K\|_F \leq \|H\|_F \cdot \frac{1}{2} \sigma_{\min}^{-3} \cdot 2\sigma_{\max}\|K\|_F = \frac{\sigma_{\max}}{\sigma_{\min}^3} \|H\|_F \|K\|_F.$$

Term 2: $T_2 := K Df(A)[E_H]$ has the same bound.

Term 3: $T_3 := Y D^2f(A)[E_K, E_H]$.

$$\|T_3\|_F \leq \|Y\|_2 \|D^2f(A)\|_{\text{op}} \|E_K\|_F \|E_H\|_F \leq \sigma_{\max} \cdot \frac{3}{4} \sigma_{\min}^{-5} \cdot (2\sigma_{\max} \|K\|_F)(2\sigma_{\max} \|H\|_F),$$

so

$$\|T_3\|_F \leq 3 \frac{\sigma_{\max}^3}{\sigma_{\min}^5} \|H\|_F \|K\|_F.$$

Term 4: $T_4 := Y Df(A)[G(H, K)]$.

$$\|T_4\|_F \leq \|Y\|_2 \|Df(A)\|_{\text{op}} \|G(H, K)\|_F \leq \sigma_{\max} \cdot \frac{1}{2} \sigma_{\min}^{-3} \cdot 2\|H\|_F \|K\|_F,$$

so

$$\|T_4\|_F \leq \frac{\sigma_{\max}}{\sigma_{\min}^3} \|H\|_F \|K\|_F.$$

Summing,

$$\|D^2 P_{\mathcal{M}}(Y)[H, K]\|_F \leq \left(3 \frac{\sigma_{\max}}{\sigma_{\min}^3} + 3 \frac{\sigma_{\max}^3}{\sigma_{\min}^5} \right) \|H\|_F \|K\|_F.$$

Thus

$$\|D^2 P_{\mathcal{M}}(Y)\|_{\text{op}} \leq 3 \frac{\sigma_{\max}}{\sigma_{\min}^3} + 3 \frac{\sigma_{\max}^3}{\sigma_{\min}^5}.$$

4. Specialization to $Y \in B(\mathcal{M}, r)$. If $Y \in B(\mathcal{M}, r)$, there exists $X \in M$ with $\|Y - X\|_F \leq r$, and hence $\|Y - X\|_2 \leq r$. By Weyl's inequality, for each singular value,

$$|\sigma_i(Y) - \sigma_i(X)| \leq \|Y - X\|_2 \leq r.$$

Since $\sigma_i(X) = 1$ for $X \in M$, we obtain

$$1 - r \leq \sigma_{\min}(Y) \leq \sigma_{\max}(Y) \leq 1 + r.$$

Therefore, for $Y \in B(\mathcal{M}, r)$,

$$\|D^2 P_{\mathcal{M}}(Y)\|_{\text{op}} \leq 3 \frac{1+r}{(1-r)^3} + 3 \frac{(1+r)^3}{(1-r)^5} =: C(r),$$

so $B(r) \leq C(r)$ as claimed.

Finally, for $r = \frac{1}{5}$ we have

$$\sigma_{\min}(Y) \geq \frac{4}{5}, \quad \sigma_{\max}(Y) \leq \frac{6}{5},$$

so

$$C\left(\frac{1}{5}\right) = 3 \frac{6/5}{(4/5)^3} + 3 \frac{(6/5)^3}{(4/5)^5} = \frac{225}{32} + \frac{2025}{128} = \frac{2925}{128} < 25.$$

This yields $B(1/5) \leq 2925/128 < 25$, and we can take $B_* = 25$ on $B(M, 1/5)$. \square

Proof of Proposition 4.3. By hypothesis, ∇f is L_f -Lipschitz on \mathcal{M} and bounded by G , so item (1) of Assumption 4.1 holds with L_f and G .

The Stiefel manifold \mathcal{M} is a compact C^3 manifold of \mathbb{E} . Let $Y \in \mathbb{E}$ be of full rank, then its projection onto \mathcal{M} is given (uniquely) by $P_{\mathcal{M}}(Y) = Y(Y^\top Y)^{-1/2}$, which is C^2 . By Wyle's inequality, any matrix in $B(M, 2/5)$ is of full rank. Thus, according to (Federer, 1959, 4.8 Theorem) (or, see (Clarke et al., 1995, Theorem 4.8)), $P_{\mathcal{M}}$ is 2-Lipschitz in $B(M, 1/5)$. It follows that $\|DP_{\mathcal{M}}(x)\|_{\text{op}} \leq 2$ for all $x \in B(M, 1/5)$. Therefore, item (2) of Assumption 4.1 holds with $r = 1/5$.

Lemma A.3 gives an explicit formula for $D^2P_{\mathcal{M}}$ and shows that, for any $Y \in B(M, 1/5)$, the singular values of Y satisfy

$$\frac{4}{5} \leq \sigma_{\min}(Y) \leq \sigma_{\max}(Y) \leq \frac{6}{5},$$

and consequently

$$\|D^2P_{\mathcal{M}}(Y)\|_{\text{op}} \leq 3 \frac{\sigma_{\max}(Y)}{\sigma_{\min}(Y)^3} + 3 \frac{\sigma_{\max}(Y)^3}{\sigma_{\min}(Y)^5} \leq \frac{2925}{128} < 25.$$

Hence

$$B_* := \sup_{x \in B(M, 1/5)} \|D^2P_{\mathcal{M}}(x)\|_{\text{op}} \leq \frac{2925}{128} < 25.$$

By the fundamental theorem of calculus along segments,

$$\|DP_{\mathcal{M}}(x) - DP_{\mathcal{M}}(x')\|_{\text{op}} \leq B_* \|x - x'\|_{\mathbb{E}}, \quad \forall x, x' \in B(M, 1/5).$$

Thus, item (3) of Assumption 4.1 follows by plugging these estimates into the computation in (17). \square

A.3. Proof of Lemma 4.4

Proof. Since $\|d\| \leq r$, we have $x + d \in B(x, r)$. By L -smoothness of $f \circ P_{\mathcal{M}}$, it holds that

$$f \circ P_{\mathcal{M}}(x + d) \leq f(x) + \langle \nabla(f \circ P_{\mathcal{M}})(x), d \rangle + \frac{L}{2} \|d\|_{\mathbb{E}}^2.$$

It remains to show that $\nabla(f \circ P_{\mathcal{M}}) = \nabla_{\mathcal{M}} f(x)$. Since both f and $P_{\mathcal{M}}$ are continuously differentiable at x , by chain rule,

$$\nabla(f \circ P_{\mathcal{M}}) = DP_{\mathcal{M}}(x) \nabla f(P_{\mathcal{M}}(x)) = P_{T_x \mathcal{M}} \nabla f(x) = \nabla_{\mathcal{M}} f(x).$$

Above, we used Theorem A.1 and the definition of Riemannian gradient. \square

A.4. Proof of Theorem 4.5

Proof. We denote the search direction at iteration t by

$$d_t := \text{LMO}_{\|\cdot\|}(\nabla_{\mathcal{M}} f(x_t)),$$

where $\|d_t\| = 1$. By Lemma 4.4, we have

$$\begin{aligned} f(x_{t+1}) &= f \circ P_{\mathcal{M}}(x_t + \alpha_t d_t) \\ &\leq f(x_t) + \alpha_t \langle \nabla_{\mathcal{M}} f(x_t), d_t \rangle + \frac{L}{2} \alpha_t^2 N^2 \|d_t\|^2 \\ &= f(x_t) - \alpha_t \|\nabla_{\mathcal{M}} f(x_t)\|_* + \frac{L}{2} \alpha_t^2 N^2. \end{aligned} \tag{18}$$

Rearranging and telescoping for $t = 0, \dots, T-1$ yields

$$\sum_{t=0}^{T-1} \alpha_t \|\nabla_{\mathcal{M}} f(x_t)\|_* \leq f(x_0) - f(x_T) + \frac{LN^2}{2} \sum_{t=0}^{T-1} \alpha_t^2 \leq \Delta + \frac{LN^2}{2} \sum_{t=0}^{T-1} \alpha_t^2 \tag{19}$$

for any $\Delta \geq f(x_0) - \inf_{x \in \mathcal{M}} f(x)$. To prove the second part of the theorem, let $T \geq \frac{2\Delta}{r^2 LN^2}$ and $\alpha_0 = \dots = \alpha_{T-1} = \sqrt{\frac{2\Delta}{TLN^2}} =: \alpha \in (0, r]$. Plugging this choice to (19), we have

$$\min_{y=0, \dots, T-1} \|\nabla_{\mathcal{M}} f(x_t)\|_* \leq \frac{1}{T} \sum_{t=0}^{T-1} \|\nabla_{\mathcal{M}} f(x_t)\|_* \leq \frac{\Delta}{\alpha T} + \frac{LN^2 \alpha}{2} = \sqrt{\frac{2\Delta LN^2}{T}}.$$

\square

A.5. Proof of Theorem 4.8

Proof. Denote by

$$d_t := \text{LMO}_{\|\cdot\|}(P_{T_{x_t}\mathcal{M}}(m_t))$$

the search direction returned by the linear minimization oracle. Let $(x_t)_{t \in \mathbb{N}}$ be a realization of Algorithm 2 with step sizes $(\alpha_t)_{t \in \mathbb{N}} \subset (0, r]$ and momentum parameter $\beta \in [0, 1)$. By Lemma 4.4, we have

$$\begin{aligned} f(x_{t+1}) &= f \circ P_{\mathcal{M}}(x_t + \alpha_t d_t) \\ &\leq f(x_t) + \alpha_t \langle \nabla_{\mathcal{M}} f(x_t), d_t \rangle + \frac{L}{2} \alpha_t^2 N^2 \|d_t\|^2. \end{aligned}$$

Using the identity $\nabla_{\mathcal{M}} f(x_t) = P_{T_{x_t}\mathcal{M}}(\nabla f(x_t))$, the definition of d_t , and the fact that $\|d_t\| \leq 1$, we obtain

$$\begin{aligned} f(x_{t+1}) &\leq f(x_t) + \alpha_t \langle P_{T_{x_t}\mathcal{M}}(m_t), d_t \rangle + \alpha_t \langle \nabla_{\mathcal{M}} f(x_t) - P_{T_{x_t}\mathcal{M}}(m_t), d_t \rangle + \frac{L}{2} \alpha_t^2 N^2 \\ &\leq f(x_t) - \alpha_t \|P_{T_{x_t}\mathcal{M}}(m_t)\|_* + \alpha_t \|\nabla_{\mathcal{M}} f(x_t) - P_{T_{x_t}\mathcal{M}}(m_t)\|_* + \frac{L}{2} \alpha_t^2 N^2 \\ &\leq f(x_t) - \alpha_t \|\nabla_{\mathcal{M}} f(x_t)\|_* + 2\alpha_t \|\nabla_{\mathcal{M}} f(x_t) - P_{T_{x_t}\mathcal{M}}(m_t)\|_* + \frac{L}{2} \alpha_t^2 N^2. \end{aligned}$$

By the fact that $\|d\|_* = \max_{\|u\| \leq 1} \langle d, u \rangle \leq \|d\|_{\mathbb{E}} \|u\|_{\mathbb{E}} \leq N \|d\|_{\mathbb{E}}$ and the contractivity of $P_{T_{x_t}\mathcal{M}}$ in $\|\cdot\|_{\mathbb{E}}$, this gives

$$f(x_{t+1}) \leq f(x_t) - \alpha_t \|\nabla_{\mathcal{M}} f(x_t)\|_* + 2\alpha_t N \|\nabla f(x_t) - m_t\|_{\mathbb{E}} + \frac{L}{2} \alpha_t^2 N^2.$$

To bound $\|\nabla f(x_t) - m_t\|_{\mathbb{E}}$, we introduce the auxiliary sequence $(C_t)_{t \in \mathbb{N}}$ defined by $C_0 := \nabla f(x_0)$ and, for $t > 0$,

$$C_t := \beta C_{t-1} + (1 - \beta) \nabla f(x_t) = (1 - \beta) \sum_{i=1}^t \beta^{t-i} \nabla f(x_i) + \beta^t \nabla f(x_0).$$

By the triangle inequality,

$$\|\nabla f(x_t) - m_t\|_{\mathbb{E}} \leq \|\nabla f(x_t) - C_t\|_{\mathbb{E}} + \|C_t - m_t\|_{\mathbb{E}}. \quad (20)$$

For the first term in (20), we have

$$\begin{aligned} \|\nabla f(x_t) - C_t\|_{\mathbb{E}} &= \|\nabla f(x_t) - (\beta C_{t-1} + (1 - \beta) \nabla f(x_t))\|_{\mathbb{E}} \\ &= \beta \|\nabla f(x_t) - C_{t-1}\|_{\mathbb{E}} \\ &\leq \beta \|\nabla f(x_{t-1}) - C_{t-1}\|_{\mathbb{E}} + \beta \|\nabla f(x_{t-1}) - \nabla f(x_t)\|_{\mathbb{E}} \\ &\leq \beta \|\nabla f(x_{t-1}) - C_{t-1}\|_{\mathbb{E}} + \beta L \|x_{t-1} - x_t\|_{\mathbb{E}} \\ &\leq \beta \|\nabla f(x_{t-1}) - C_{t-1}\|_{\mathbb{E}} + 2\beta L \alpha_t \|d_t\|_{\mathbb{E}} \\ &\leq \beta \|\nabla f(x_{t-1}) - C_{t-1}\|_{\mathbb{E}} + 2\beta L \alpha_t N. \end{aligned}$$

Above, we used the L -smoothness of f and 2-Lipschitz continuity of $P_{\mathcal{M}}$. Let $\bar{\alpha} := \max_{i=0, \dots, t} \alpha_i$, the above yields

$$\|\nabla f(x_t) - C_t\|_{\mathbb{E}} \leq \beta \|\nabla f(x_{t-1}) - C_{t-1}\|_{\mathbb{E}} + 2\beta L \bar{\alpha} N.$$

Iterating this recursion and using $C_0 = \nabla f(x_0)$ gives

$$\begin{aligned} \|\nabla f(x_t) - C_t\|_{\mathbb{E}} &\leq \beta^t \|\nabla f(x_0) - C_0\|_{\mathbb{E}} + 2\beta L \bar{\alpha} N \sum_{i=0}^{t-1} \beta^i \\ &= 2\beta L \bar{\alpha} N \sum_{i=0}^{t-1} \beta^i \leq \frac{2N \beta L \bar{\alpha}}{1 - \beta}. \end{aligned}$$

For the second term in (20), note that the momentum terms satisfy

$$m_t = \beta m_{t-1} + (1 - \beta)g_t = (1 - \beta) \sum_{i=1}^t \beta^{t-i} g_i + \beta^t g_0.$$

Therefore,

$$\begin{aligned} \mathbb{E}\|C_t - m_t\|_{\mathbb{E}} &\leq (1 - \beta) \mathbb{E}\left[\left\|\sum_{i=1}^t \beta^{t-i} (g_i - \nabla f(x_i))\right\|_{\mathbb{E}}\right] + \beta^t \mathbb{E}\|g_0 - \nabla f(x_0)\|_{\mathbb{E}} \\ &\leq (1 - \beta) \sqrt{\mathbb{E}\left[\left\|\sum_{i=1}^t \beta^{t-i} (g_i - \nabla f(x_i))\right\|_{\mathbb{E}}^2\right]} + \beta^t \sqrt{\mathbb{E}\|g_0 - \nabla f(x_0)\|_{\mathbb{E}}^2} \\ &\leq (1 - \beta) \sqrt{\sum_{i=1}^t \beta^{2(t-i)} \sigma^2 + \beta^t \sigma^2} \\ &\leq \left(\sqrt{\frac{1-\beta}{1+\beta}} + \beta^t\right) \sigma, \end{aligned}$$

where we used Assumption 4.7 for the stochastic gradients $(g_t)_{t \in \mathbb{N}}$.

Combining the two bounds, we obtain

$$\begin{aligned} \mathbb{E}[f(x_{t+1}) - f(x_t)] &\leq -\alpha_t \mathbb{E}\|\nabla_{\mathcal{M}} f(x_t)\|_* + 2\alpha_t N \mathbb{E}\|\nabla f(x_t) - m_t\|_{\mathbb{E}} + \frac{L}{2} \alpha_t^2 N^2 \\ &\leq -\alpha_t \mathbb{E}\|\nabla_{\mathcal{M}} f(x_t)\|_* + 2\alpha_t N \left(\frac{2N\beta L \bar{\alpha}}{1-\beta} + \left(\sqrt{\frac{1-\beta}{1+\beta}} + \beta^t\right) \sigma\right) + \frac{L}{2} \alpha_t^2 N^2. \end{aligned}$$

Summing this inequality from $t = 0$ to $T - 1$ and telescoping the left-hand side, we obtain

$$\sum_{t=0}^{T-1} \alpha_t \mathbb{E}\|\nabla_{\mathcal{M}} f(x_t)\|_* \leq \mathbb{E}[f(x_0) - f(x_T)] + 2N \sum_{t=0}^{T-1} \left(\frac{2N\beta L \bar{\alpha}}{1-\beta} + \left(\sqrt{\frac{1-\beta}{1+\beta}} + \beta^t\right) \sigma\right) \alpha_t + \frac{LN^2}{2} \sum_{t=0}^{T-1} \alpha_t^2. \quad (21)$$

This gives the first claim of the theorem.

We now specialize to the constant step size regime. Assume $\alpha_t = \alpha$ for all t and set

$$\Delta \geq f(x_0) - \inf_{x \in \mathcal{M}} f(x) \quad \text{so that} \quad \mathbb{E}[f(x_0) - f(x_T)] \leq \Delta.$$

Dividing (21) by $T\alpha$ yields

$$\begin{aligned} \frac{1}{T} \sum_{t=0}^{T-1} \mathbb{E}\|\nabla_{\mathcal{M}} f(x_t)\|_* &\leq \frac{\Delta}{\alpha T} + 2N \left(\frac{2N\beta L \alpha}{1-\beta} + \left(\sqrt{\frac{1-\beta}{1+\beta}} + \frac{1}{(1-\beta)T}\right) \sigma\right) + \frac{LN^2 \alpha}{2} \\ &= \frac{\Delta}{\alpha T} + \frac{\alpha LN^2}{2} \left(\frac{8\beta}{1-\beta} + 1\right) + 2N \sigma \left(\sqrt{\frac{1-\beta}{1+\beta}} + \frac{1}{(1-\beta)T}\right). \end{aligned} \quad (22)$$

We first choose α as

$$\alpha := \sqrt{\frac{2\Delta}{LN^2 T \left(\frac{8\beta}{1-\beta} + 1\right)}}. \quad (23)$$

A direct computation shows that the first two terms on the right-hand side of (22) then combine into

$$\frac{\Delta}{\alpha T} + \frac{\alpha LN^2}{2} \left(\frac{8\beta}{1-\beta} + 1\right) = N \sqrt{\frac{2L\Delta}{T} \left(\frac{8\beta}{1-\beta} + 1\right)},$$

so that

$$\frac{1}{T} \sum_{t=0}^{T-1} \mathbb{E}[\|\nabla_{\mathcal{M}} f(x_t)\|_*] \leq N \sqrt{\frac{2L\Delta}{T} \left(\frac{8\beta}{1-\beta} + 1 \right)} + 2N\sigma \left(\sqrt{\frac{1-\beta}{1+\beta}} + \frac{1}{(1-\beta)T} \right). \quad (24)$$

We now choose β as a function of T by setting

$$\beta := 1 - T^{-1/2}, \quad \delta := 1 - \beta = T^{-1/2}.$$

Then

$$\frac{8\beta}{1-\beta} + 1 = \frac{8(1-\delta)}{\delta} + 1 = 8\sqrt{T} - 7 \leq 8\sqrt{T},$$

and therefore, from (24),

$$N \sqrt{\frac{2L\Delta}{T} \left(\frac{8\beta}{1-\beta} + 1 \right)} \leq N \sqrt{\frac{2L\Delta}{T} \cdot 8\sqrt{T}} = 4N\sqrt{L\Delta}T^{-1/4}.$$

Moreover,

$$\sqrt{\frac{1-\beta}{1+\beta}} = \sqrt{\frac{\delta}{2-\delta}} \leq \sqrt{\delta} = T^{-1/4} \quad \text{and} \quad \frac{1}{(1-\beta)T} = \frac{1}{\delta T} = T^{-1/2}.$$

Hence

$$2N\sigma \left(\sqrt{\frac{1-\beta}{1+\beta}} + \frac{1}{(1-\beta)T} \right) \leq 2N\sigma(T^{-1/4} + T^{-1/2}) \leq 4N\sigma T^{-1/4}$$

for all $T \geq 1$. Plugging these estimates into (24), we obtain

$$\frac{1}{T} \sum_{t=0}^{T-1} \mathbb{E}[\|\nabla_{\mathcal{M}} f(x_t)\|_*] \leq 4N(\sqrt{L\Delta} + \sigma)T^{-1/4}. \quad (25)$$

Finally, we verify that the chosen step size satisfies $\alpha \leq r$. For our choice of β ,

$$\frac{8\beta}{1-\beta} + 1 = 8\sqrt{T} - 7,$$

so (23) becomes

$$\alpha = \sqrt{\frac{2\Delta}{LN^2T(8\sqrt{T}-7)}}.$$

For $T \geq 4$ we have $\sqrt{T} \geq 2$ and hence $8\sqrt{T} - 7 \geq 4\sqrt{T}$, which implies

$$\alpha^2 = \frac{2\Delta}{LN^2T(8\sqrt{T}-7)} \leq \frac{2\Delta}{LN^2T \cdot 4\sqrt{T}} = \frac{\Delta}{2LN^2T^{3/2}}.$$

A sufficient condition for $\alpha \leq r$ is therefore

$$\frac{\Delta}{2LN^2T^{3/2}} \leq r^2 \iff T^{3/2} \geq \frac{\Delta}{2LN^2r^2}.$$

Define

$$T_0 := \max \left\{ 4, \left(\frac{\Delta}{2LN^2r^2} \right)^{2/3} \right\}.$$

Then for all integers $T \geq T_0$ we have $\alpha \leq r$, so the above choice of $(\alpha_t)_{t=0}^{T-1}$ and β is admissible and (25) holds. Since

$$\min_{t=0, \dots, T-1} \mathbb{E}[\|\nabla_{\mathcal{M}} f(x_t)\|_*] \leq \frac{1}{T} \sum_{t=0}^{T-1} \mathbb{E}[\|\nabla_{\mathcal{M}} f(x_t)\|_*],$$

the claimed bound in the theorem follows. \square

B. Supplementary experimental results

B.1. Principal component analysis (PCA)

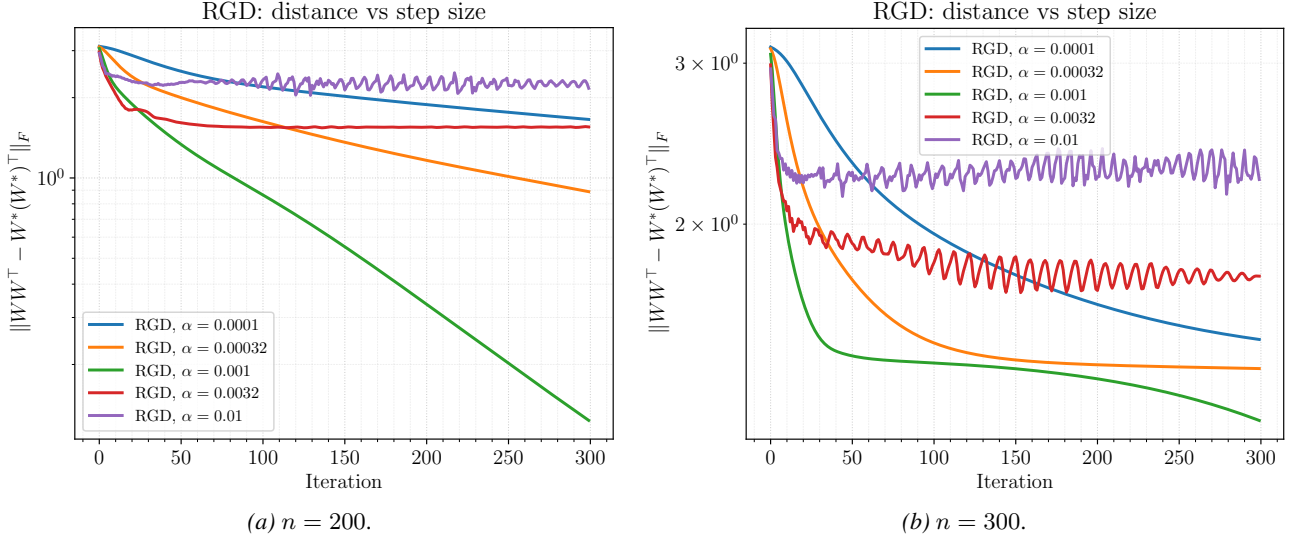


Figure 4. PCA with RGD under different constant step sizes ($p = 5, d = 1000$). The figure shows the convergence behavior of RGD with varying constant step sizes, where $\alpha = 0.001$ provides the best convergence rate, which is used in PCA experiments (Figure 2).

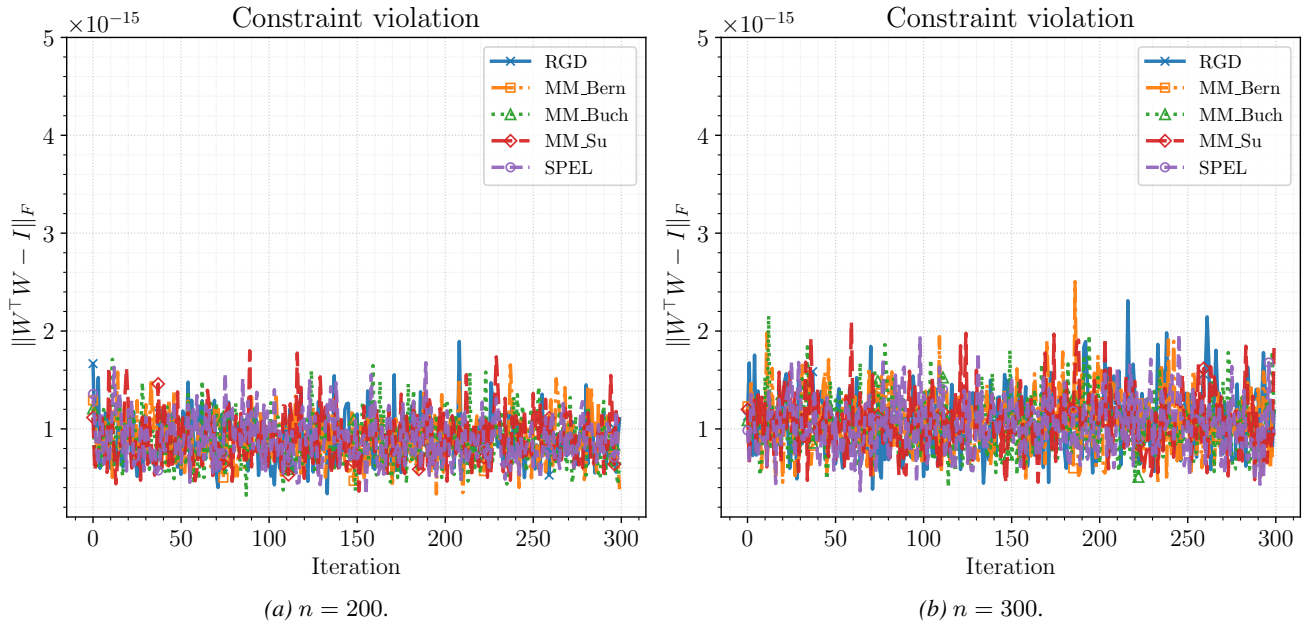
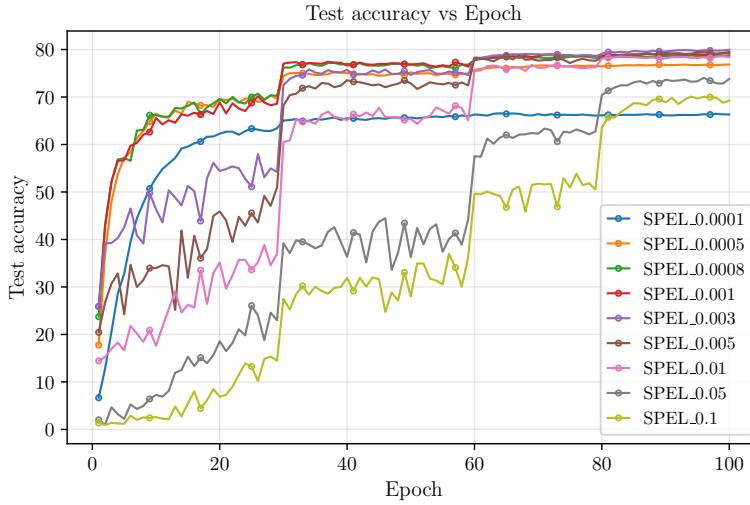


Figure 5. Orthogonality constraint violation $\|WW^T - I\|_F$ under the msign operation using the Polar Express algorithm (Amsel et al., 2025) with eight iterations. Numerical precision is set to float64. The experiment shows that all algorithms maintain high precision in satisfying the orthogonality constraint at each iteration, validating the feasibility of using the Polar Express approximation as a projection operator onto the Stiefel manifold without relying on SVD.

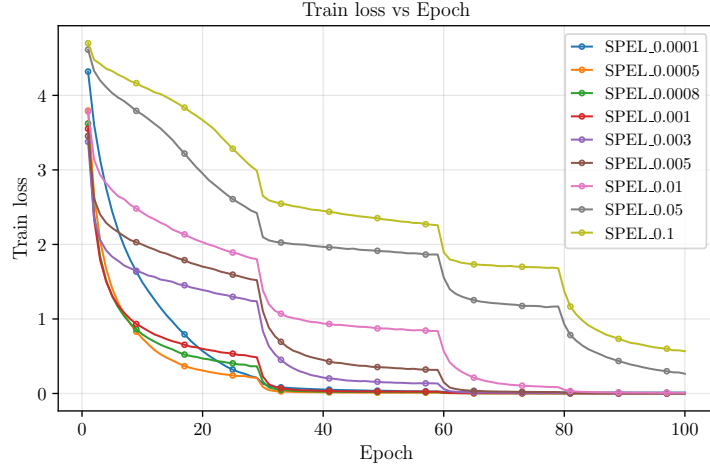
B.2. Orthogonality in CNNs

Table 5. Comparison of different retraction operators for Stiefel-constrained optimization. We evaluate Riemannian SGD with momentum ($lr_s = 0.2$, $lr_e = 0.01$) and Riemannian Adam ($lr_s = 0.4$, $lr_e = 0.01$), each equipped with various retraction operators: the standard Cayley retraction (Li et al., 2020), the CANS retraction (Grishina et al., 2025), and the Polar Express retraction (Amsel et al., 2025). Polar-Express consistently achieves the lowest per-epoch training time while maintaining comparable classification accuracy compared to both Riemannian SGD and Riemannian Adam.

Optimizer	Retraction	Accuracy (%)	Time per epoch (s)
RSGD	Cayley	72.19	50.15
RSGD	CANS	71.98	42.30
RSGD	Polar Express	72.10	35.07
RAdam	Cayley	77.48	50.59
RAdam	CANS	77.28	42.93
RAdam	Polar Express	77.73	35.36



(a) Test accuracy under different learning rates.



(b) Training loss under different learning rates.

Figure 6. Optimizing the Learning Rate Ratio for SPEL on CIFAR-100. This figure investigates the optimal learning rate ratio for SPEL by varying lr_s while fixing $lr_e = 0.001$. The figure shows the test accuracy and training loss as functions of training epochs for different values of lr_s . The results indicate that $lr_s = 0.003$ achieves the best performance, resulting in an optimal learning rate ratio of $lr_s/lr_e = 3$.

B.3. LLM adapter tuning: StelLA with SPEL

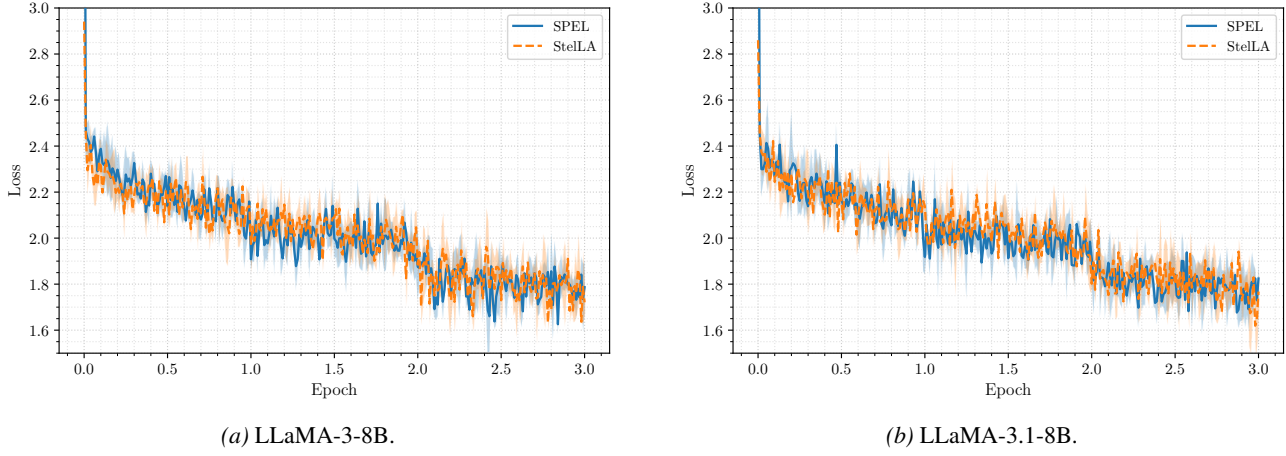


Figure 7. Fine-tuning loss for LLaMA-3-8B and LLaMA-3.1-8B (over 3 epochs) across 3 runs. The two figures compare the performance of SPEL with the algorithm from the StelLA framework (Li et al., 2025).